CRACK ARREST METHODOLOGY FOR THICK SECTIONS

George T. Hahn*, R. G. Hoagland*, and R. D. Cheverton**

*Vanderbilt University, Nashville, Tennessee
**Oak Ridge National Laboratores, Oak Ridge, Tennessee

ABSTRACT

The magnitude of dynamic effects associated with crack arrest are related to the conservation of kinetic energy in the structure and the nature of the fast fracture toughness (K_{ID}) -crack velocity curve of the material. Recent findings of a 29 laboratory cooperative test program performed on compact specimens of A533B steel, and measurements of the run arrest events produced in large thermally shocked cylinders, which show that static analyses of arrest are valid in these cases, are consistent with this view.

KEYWORDS

Crack arrest, crack arrest toughness, fast fracture toughness, crack velocity, cooperative test program, A533B steel, thermal shock, cylinders.

INTRODUCTION

This paper reviews advances toward a fracture mechanics methodology for predicting crack arrest in thick sections. The paper examines: (i) static and dynamic analysis approaches, (ii) the progress toward arrest toughness testing standards, and (iii) the implications of large scale test experience from thermally shocked cylinders of a nuclear grade of steel.

ANALYSES OF CRACK ARREST

Analyses of crack arrest of the type illustrated in Fig. 1 are complicated by a number of "dynamic effects" which are absent at the onset of crack extension. One of these is the variation of K_{ID} with crack velocity* (see Fig. 2). A

* The quantity K_{ID}, the fast fracture toughness, is the running crack equivalent of K_{IC} . The minimum value of K_{ID} is designated K_{Im}, the crack arrest toughness. The K_{ID}-crack velocity curve (and K_{Im}) are here regarded as geometry independent material properties that enter into dynamic LEFM criteria: for propagation $K_I = K_{ID}(v)$ and arrest $K_I < K_{Im}$[4], although the question of geometry dependence is still an unsettled issue[10].

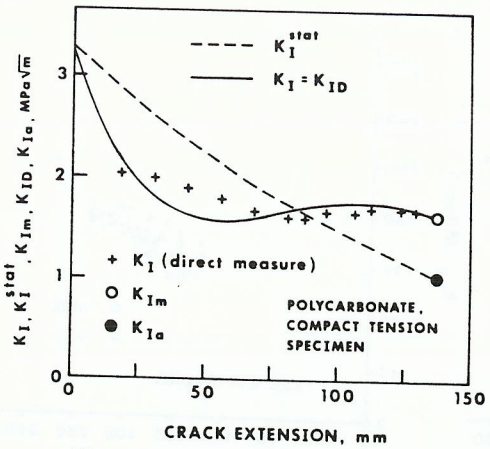

Fig. 1. Finite element analysis of run-arrest event after Kobayashi (1)

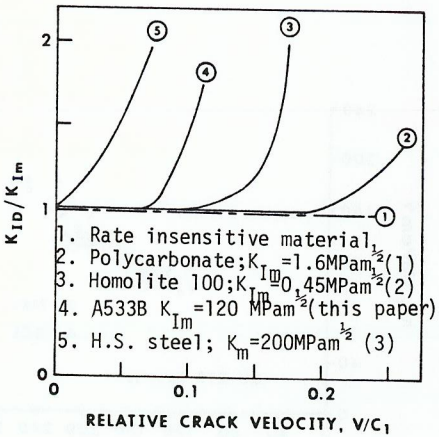

Fig. 2. K_{ID}-crack velocity curves at room temp.

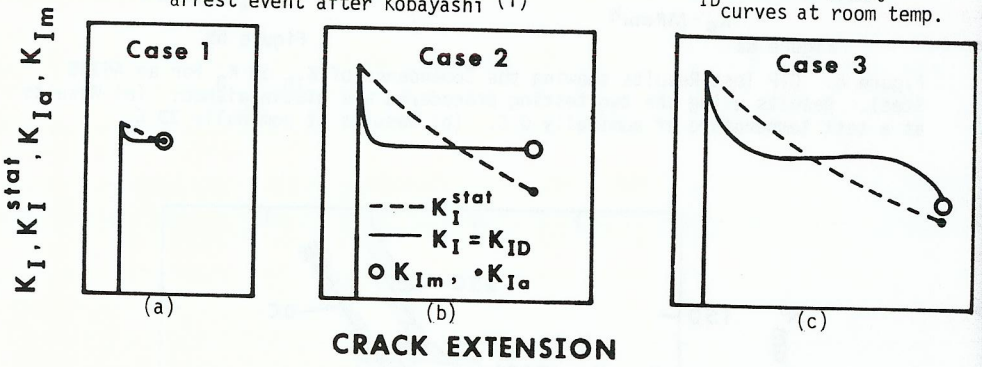

Fig. 3. Effect of kinetic energy conservation on stress intensity at arrest: (a) Case 1, (b) Case 2, (c) Case 3.

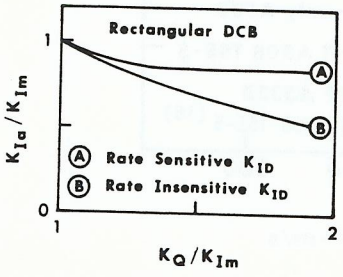

Fig. 4. Effect of K_{ID}-velocity curve on departures from static solution at arrest. (8)

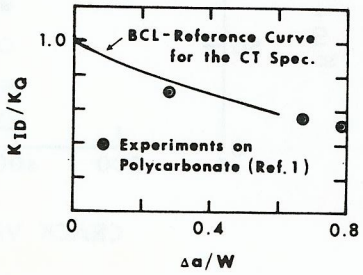

Fig. 5. Comparison of dynamic analysis (BCL Reference Curve) with experiments of Kobayashi et al. (1)

second dynamic effect is the departure of K_I, the instantaneous value of the stress intensity factor of a propagating or arresting crack, from K_I^{stat}, the static equilibrium value for a stationary crack of the same length. The departure is caused by the inertia of the cracked body and can lead to the conversion of kinetic energy to fracture energy causing the crack to over-shoot, i.e. propagate while $K_I^{stat} < K_{ID}$ as illustrated in Figure 1. The value of K_I^{stat} at arrest is usually designated K_{Ia}; the difference between K_{Im} and K_{Ia} is the departure from static equilibrium, which is about 50% for the example in Figure 1. A third dynamic effect is the oscillation of the cracked component immediately after arrest as a result of kinetic energy trapped in the body. (5)

The magnitude of these dynamic effects, particularly the difference between K_{Im} and K_{Ia}, depends on the relative amount of kinetic energy that is conserved, i.e., converted to fracture energy. Three special cases, illustrated schematically in Fig. 3 are instructive.

Case 1. No Conservation

There is essentially no conservation when the amount of kinetic energy imparted to the fracturing body is small relative to the fracture energy and/or becomes widely dispersed. The overshoot and departure from static equilibrium at arrest are then negligible, as illustrated in Fig. 3a. These conditions are obtained for a crack jump that is small relative to the dimensions of the cracked body. The crack jumps produced in the thermal shock experiments discussed later fall into this category.

Case 2. Partial Conservation

A large part of the imparted kinetic energy (~70% in the case of Fig. 1) is conserved when a relatively large amount of kinetic energy is imparted and the K_{ID}-value is rate insensitive (see Curve 1 in Fig.2). This is the case because there is little opportunity for damping in the short time intervals involved here. (6) As a result, substantial overshoot and departure from equilibrium are then obtained (Fig. 3b). Since $K_I = K_{ID} = \text{const}$ under these conditions, K_I and K_I^{stat} must diverge as shown in Figs. 3b and 4. (7) Kinetic energy must be retained and large oscillations follow arrest. This case corresponds with crack jumps that are large compared with the body dimensions, such as the crack jumps produced in polycarbonate CT-specimens (1) (See Fig. 1) and araldite DCB specimens (7). Apparently, the K_{ID}-velocity curves of these materials (see Fig. 2) are sufficiently rate insensitive at low velocities to trap kinetic energy. Both finite difference and finite element calculations (1), that account for inertia and rate effects, are in good agreement with experiments (1,9) as shown in Figs. 1 and 5.

Case 3. Complete Conservation

Nearly complete conservation is possible when a relatively large amount of kinetic energy is coupled with a strong rate sensitive K_{ID} like curve 5 in Fig. 2. In this case, overshoot is accompanied by a progressive decrease of K_I as the crack decelerates. Fig. 3c and the calculations of Fig. 4 indicate that this combination produces more complete kinetic energy conservation prior to arrest, smaller departures from static equilibrium at arrest, and smaller oscillations after arrest (8). As a result, a static analysis of arrest assuming $K_{Ia} = K_{Im}$ may again be valid. Findings for A533B compact tension specimens discussed in the next section fit into this category.

RESULTS OF THE COOPERATIVE TEST PROGRAM

An important step toward a standardized laboratory test procedure for measuring K_{Im} was taken with the conduct of the Cooperative Test Program (CTP) under ASTM auspices. Briefly, the charge of the CTP was to critically examine procedures for measuring K_{ID} and K_{Ia} developed at Battelle Columbus Laboratories and the Materials Research Laboratories, respectively. The two procedures were applied to a common material (A533 grade B, RT_{NDT}= -40 C) in 29 laboratories each testing compact-tension type specimens for a total of 233 crack arrest tests on a single heat of A533B steel at two test temperatures: nominally 0 C. and 23 C. Earlier coordination between BCL and MRL led to two procedures which were very similar in terms of the specimen geometry and the physical conduct of the test, a fact which greatly assists direct comparison of the results. These results provide a statistically extensive crack arrest toughness data base and an opportunity to assess the significance of K_{ID} and K_{Ia} in predicting crack arrest in large structures. A more complete description of the CTP and the two test procedures as they existed at the initiation of the CTP can be found in references 9 and 11, respectively.

The CTP test results from the two procedures do not differ significantly, and two observations are particularly relevant here. The first is that K_{ID} increases approximately linearly with K_Q, the stress intensity at the onset of propagation, a feature revealed in Fig. 6. This figure shows that while the average values of the 2 procedures differ, the K_{ID}-data are members of the same group. The variation of K_{ID} with K_Q is the signature of a rate sensitive material (12). The second observation is that K_{Ia} is essentially independent of K_Q, with the average results of the two test procedures in good agreement. This latter finding is consistent with the calculations summarized in Fig. 4 for a rate sensitive material and the limited range of K_Q produced in these tests.

The rationalization of the two observations described above requires that K_{ID} increases with increasing crack velocity. The functional form of this relation is expressed graphically in Figure 7.* For both test temperatures, the toughness-velocity relation shows positive curvature and a very sharp increase in K_{ID} above ~600-700 m/s. Therefore, the propagation of cracks at velocities $\gtrsim$ 700 m/s would be difficult. At low velocities, it is significant to note that the lower bound of the K_{ID} -values (defined by the lower bound of the average of the K_{ID} data in Fig. 7) are very nearly equal to the average K_{Ia}. This is consistent with the expected approach of K_{ID} and K_{Ia} at low average crack velocities† and the validity of a

* As shown in Reference 9 and 12, the dynamic calculations for the CT specimen lead to a functional description of $v=f(\Delta a/w)$ and $K_D/K_Q=g(\Delta a/w)$ where v is the crack velocity and f and g are functions of $\Delta a/w$ deduced from a series of dynamic calculations. Combining these expressions with the CTP results given in Fig. 6 leads to Fig. 7.

† K_{Ia} may appear to exceed K_{ID} because of insufficient loading machine stiffness. This follows because K_{ID} is derived using δ_o the crack mouth displacement at initiation, while K_{Ia} is computed from δ_a, the displacement at arrest. Lack of testing machine stiffness causes $\delta_a > \delta_o$ by a significant amount. In CTP $\delta_a = 1.095\ \delta_o$, on average.

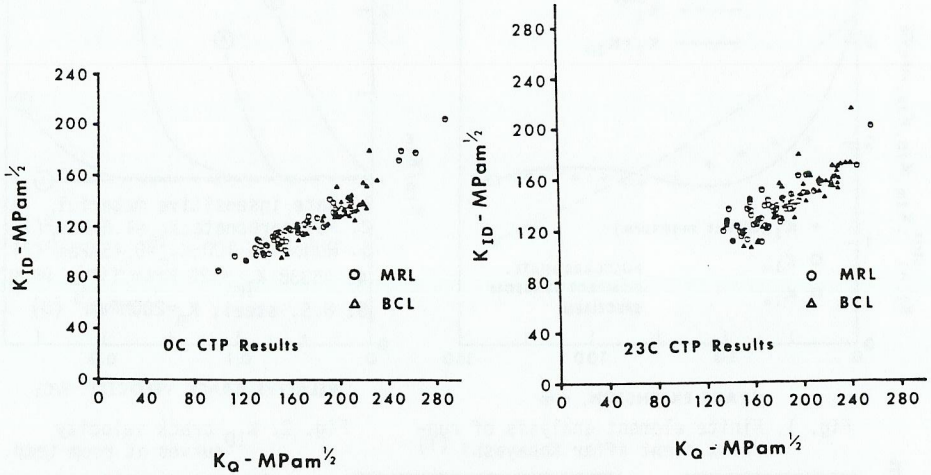

Figure 6a Figure 6b

Figure 6. CTP Test Results showing the Dependence of K_{ID} on K_Q for an A533B Steel. Results using the two testing procedures are distinguished. (a) Results at a test temperature of nominally 0 C. (b) Results at nominally 23 C.

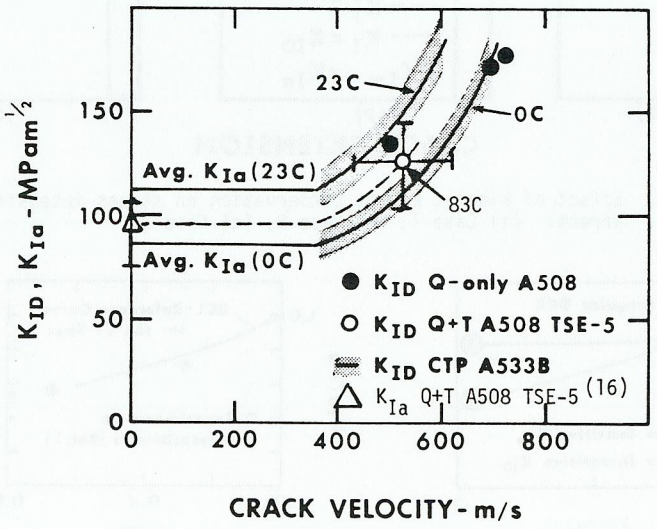

Figure 7. The Crack Velocity Dependence of K_{ID} Derived from the CTP Results. The shaded bands identify the scatter band. Also shown are the average K_{Ia} from the CTP, K_{ID} data for quenched-only A508 and quenched and tempered A508 (TSE-5 material). (16) The dashed line shows a possible crack velocity dependence for TSE-5 material. The brackets indicate the range of the measurements.

static analysis for Case 3-type run arrest events as discussed in the preceeding section. Very limited crack arrest measurements of K_{ID} on a quenched-only A508 taken from TSE-4 are also shown in Figure 7. These results display a velocity dependence with a character similar to the CTP A533B material. We present this data because it supports the assumption that the K_{ID} of the Q and T A508 material in TSE-5 obeys a similar velocity dependence. This is fairly reasonable considering that the RT_{NDT} of TSE-5 (+66C) material falls between the CTP material (-40C) and TSE-4 material (200C).

APPLICATION TO THERMAL-SHOCK EXPERIMENTS

Crack arrest methodologies are being used to analyze crack arrest events in thick walled steel cylinders that are subjected to severe thermal-shock loadings. Five thermal shock experiments have been conducted so far as a part of the program at Oak Ridge National Laboratory (ORNL)[13,14]. Two of these experiments (TSE-4 and TSE-5) are of particular interest with regard to crack arrest behavior.

For both experiments the test cylinder material was ASTM A508, class 2-chemistry steel, and the initial flaws were shallow, sharp cracks on the inner surface extending the full length of the cylinder. Dimensions for the TSE-4 cylinder were 533-mm OD x 152-mm wall x 914-mm length, and for TSE-5 they were 991-mm OD x 152-mm wall x 1220-mm length; the initial flaw depths were 11 mm and 15 mm, respectively. Special heat treatments provided rather high transition temperatures; a quench-only treatment (quenched in water from 871°C) was used for TSE-4, and the TSE-5 cylinder was tempered for four hours at 613°C. The thermal shocks were achieved by first heating the test cylinders to a uniform temperature (291°C for TSE-4 and 96°C for TSE-5) and then rapidly cooling the inner surface with a water-alcohol mixture at -25°C for TSE-4 and liquid nitrogen (-196°C) for TSE-5.

During TSE-4 a single initiation-arrest event took place at a time of 150s into the transient and resulted in a uniform radial extension of the flaw of 12 mm for a total final depth of 23 mm. A comparison of the calculated K_I values (based on the measured radial temperature distribution), corresponding to the TSE-4 initiation and arrest events, with the K_{Ia} and K_{Ic} data obtained using DCB and CT specimens is shown in Figure 8. It is observed that the K_{Ia} data fall below the K_{Ic} data, as would be expected, and the K_{Ia} value deduced from TSE-4 agrees very well with the lab K_{Ia} data. This latter condition indicates that at least for the shallow event involved a static analysis is adequate for predicting the crack-jump distance.

During the TSE-5 thermal transient, there was a series of three initiation-arrest events as illustrated by the critical-crack-depth curves in Figure 9; data pertaining to these events are summarized in Table 1. The second initiation exhibits a high toughness relative to that for the first and third initiation events, and thus the second crack jump was considerably larger than the other two, being equal to 66 mm, or 43% of the wall thickness. Two crack-opening-displacement (COD) gages mounted on the inner surface of the cylinder were used to measure COD rate during the second crack jump; by relating crack depth to COD using a static finite element analysis [15] the COD data were used to estimate crack-tip velocity. The COD rate and thus crack-tip velocity reached a maximum immediately and then decreased continuously until arrest. (See Fig. 10). The estimated maximum crack-tip velocity was 120 m/s.

Calculated K_I values corresponding to the initiation and arrest events during TSE-5 are included in Table 1 and are plotted as a function of test temperature in

Table 1. Summary of events for TSE-5

Initiation-arrest event	1st	2nd	3rd
Time, s	105	177	205
Crack depth, mm			
Initiation	15	30	96
Arrest	30	96	122
Temperature, °C			
Initiation	−9	−3	79
Arrest	36	82	89
K_{Ic}, MN·m$^{-3/2}$	79	111	115
K_{Ia}, MN·m$^{-3/2}$	86	104	92

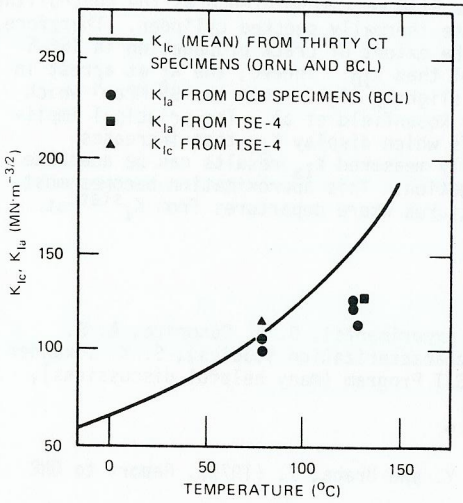

Fig. 8. K_{Ia} and K_{Ic} data for TSE-4.

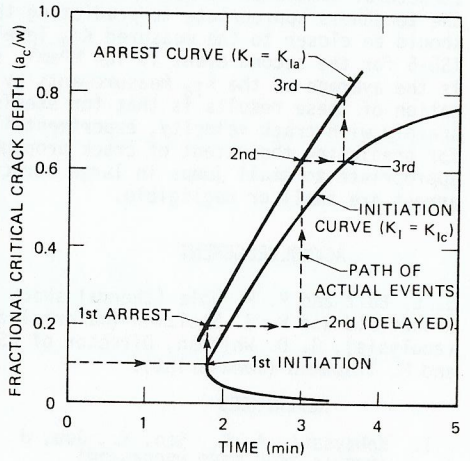

Fig. 9. Critical-crack-depth curves for TSE-5.

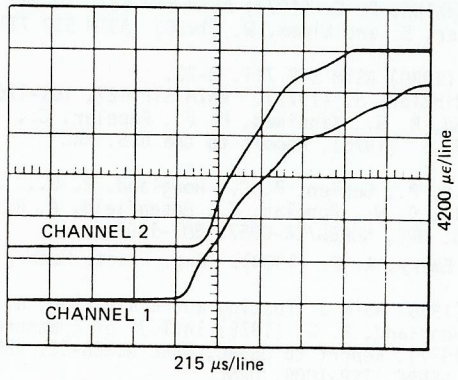

Fig. 10. COD output vs time for second crack jump during TSE-5.

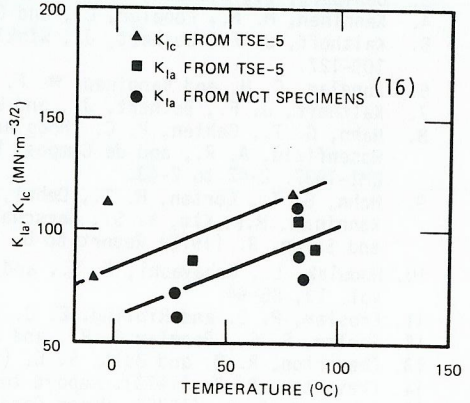

Fig. 11. K_{Ia} and K_{Ic} data for TSE-5.

Figure 11, along with K_{Ia} data obtained from wedge-loaded CT specimens similar to those employed in the CTP.[16] The K_I values corresponding to the arrest events are about equal to the lab K_{Ia} values and are about 20% below those corresponding to the initiation events.

In view of the CTP test results, a simplified interpretation of the crack jump events in TSE-5 emerges. Referring again to Figure 7, the average K_{ID} result and average estimated velocity of 550 m/s are plotted together with average K_{Ia} results for a 86 C test temperature. These results were obtained by Rosenfield et al [16] on wedge-loaded compact tension specimens machined from the TSE-5 material. The dashed line shows the expected velocity dependence of TSE-5 material. As described above, a velocity dependence of this kind leads to conditions for Case 3 behavior in which $K_{Ia} \approx K_{Im}$ in a CT specimen. The absence of a dynamic effect ($K_{Ia} = K_{Im}$) for the second, 66 mm-long crack jump of TSE-5 is regarded as evidence that a Cast 1 interpretation involving the 3110 mm circumference as the controlling structural dimension is appropriate for the thermally shocked cylinder. Therefore, the toughness appropriate to predicting the extent of crack propagation in TSE-5 should be closer to the measured K_{Ia} level than K_{ID}. Indeed, the K_I at arrest in TSE-5 for the second event is 104 MPam$^{\frac{1}{2}}$, slightly higher than the 95 MPam$^{\frac{1}{2}}$ which is the average of the K_{Ia} measurements by Rosenfield et al. The principal implication of these results is that for steels which display K_{ID} that increases sharply with crack velocity, experimentally measured K_{Ia} results can be adequate for predicting the extent of crack propagation. This approximation becomes most appropriate to small jumps in large structures where departures from K_I^{stat} at arrest are small or negligible.

ACKNOLWEDGEMENT

S. E. Bolt and P. P. Holz (thermal shock experiments), D. A. Canonico, A. R. Rosenfield and W. J. Stelzman (material characterization studies), S. K. Iskander (analysis), G. D. Whitman, Director of HSST Program (many helpful discussions), and M. Trautman (manuscript).

REFERENCES

1. Kobayashi, A. S., Seo, K., Jou, J. Y. and Uraba, Y. (1979). Report to ONR (N00014-76-C-0060 NR064-478).
2. Kobayashi, T., and Dally, J. W. (1977). ASTM STP 627, 257-273.
3. Dahlberg, L., Nilsson, F., and Brickstad, D. (1980), ASTM STP 711.
4. Kanninen, M. F., Popelar, C., and Gehlen, P. C. (1977) ASTM STP 627, 19-38.
5. Kalthoff, J. F., Beinert, J., Winkler, S. and Klemm, W. (1980) ASTM STP 711, 109-127.
6. Popelar, C. H. and Kanninen, M. F. (1980) ASTM STP 711, 3-23.
7. Kalthoff, J. F., Beinert, J., and Winkler, S. (1977). ASTM STP 627, 161-176.
8. Hahn, G. T., Gehlen, P. C. Hoagland, R. G., Kanninen, M. F., Popelar, C., Rosenfield, A. R., and de Campos, V. S (1975), Report to the U.S. NRC BMI-1937. 2-42 to 2-43.
9. Hahn, G. T., Corten, H. T., Debel, C. P., Gehlen, P. C., Hoagland, R. G., Kanninen, M.F., Kim, K. S., Marschall, C. W., Popelar, C., Rosenfield, A. R., and Simon, R. (1978) Report to U. S. NRC, NUREG/CR-0057, BMI-1995.
10. Hodulak, L., Kobayashi, A. S., and Emery, A. F. (1980). Eng. Fract. Mech., Vol. 13, 85-94.
11. Crosley, P. B. and Ripling, E. J. (1980) ASTM J. Testing and Evaluation, 8, 25.
12. Gehlen, P. C., Popelar C. H., and Hoagland, R. G. (1979) Intl.J. of Fracture 15,6
13. Cheverton, R. D. and Bolt, S. E. (1977), Report to USNRC, ORNL/NUREG-22, ORNL.
14. Cheverton, R. D. (1979). Report to USNRC, TSP-1006, ORNL.
15. Iskander, S. K. (1976). Union Carbide Nuclear Report, K/CSD/TM-2.
16. Rosenfield, A. R., Abu-Sayed, I., Gillot, R., Kanninen, M. F., Jung, R., Marschall, C. W., and Popelar, C. (1979) Report to USNRC BMI-2046.